Potential for Exciton Condensation in a Highly-Conductive Amorphous Polymer

Anna O. Schouten,[1,*] Jordan Klevens,[1,*] LeeAnn M. Sager-Smith,[1]
Jiaze Xie,[2] John S. Anderson,[2] and David A. Mazziotti[1]

[1] *Department of Chemistry and The James Franck Institute, The University of Chicago, Chicago, IL 60637*
[2] *Department of Chemistry, The University of Chicago, Chicago, IL 60637*

(Dated: Submitted August 30, 2022; Revised December 5, 2022; Revised March 10, 2023)

An outstanding challenge in synthesis and theory is to develop molecular materials at ambient conditions that exhibit highly efficient energy transfer. Here we demonstrate the potential of a recently synthesized, highly-conductive amorphous material—a nickel tetrathiafulvalene-tetrathiolate (NiTTFtt) polymer—to become an exciton condensate—a Bose-Einstein condensate of particle-hole pairs, known as excitons, that supports dissipationless flow of excitation energy. While exciton condensates have recently been realized in ordered materials, we show by advanced electronic structure calculations that this highly correlated phenomenon can potentially be realized in molecularly-tailored, amorphous materials. In contrast to the Bechgaard salts that support superconductivity at compressed geometries requiring high pressures, we show that the recently synthesized, amorphous NiTTFtt polymer exhibits the computational signature of exciton condensation at experimentally realizable geometries, occurring at ambient pressures. Results suggest that superfluidity in this system and related systems—including van der Waal structures, molecular metals with extended-TTF dithiolate ligands, and Bechgaard salts—may occur via a non-traditional excitonic mechanism tuneable according to system composition, geometry, size, and charge. This study prompts further experimental investigation of the rational design of molecularly-scaled exciton condensates with potential applications to efficient transport in technologically-relevant materials.

PACS numbers: 31.10.+z

I. INTRODUCTION

Tetrathiafulvalene (TTF) has played a central role in the development of organic conductors and superconductors. TTF is an ideal building block for conductive materials because it has inherent charge transfer abilities due to a combination of high symmetry and strong $\pi-\pi$ overlap when stacked [1]. In fact, in crystalline lattices of TTF and TTF derivatives, like $(TMTSF)_2PF_6$ — called Bechgaard salts — superconductivity can be induced with high pressures and low temperatures [1–6]. TTF structures with transition metal centers, like nickel bisdithiolene ($Ni(dmit)_2$), also exhibit conductivity and superconductivity through $\pi-\pi$ overlap and delocalization along chains [7, 8]. Moreover, transition metal complexes with TTF ligands were the first molecules found to form single-component molecular conductors [9]. Single-component molecular conductors, which, in contrast to Bechgaard salts, form highly conductive materials without a secondary molecule to facilitate charge transfer [3–6], often include transition metal centers and extended TTF-dithiolate ligands that have important conductive properties. Conductivity in single-component molecular conductors depends not only on the charge transfer capabilities of TTF, but also the strong intermolecular sulfur-sulfur interactions of the dithiolate ligands which significantly enhance conductivity. Notably Bechgaard salts, organic conductors composed of TTF derivatives, and single-component molecular conductors all have carefully ordered crystal structures which are necessary to exploit the high symmetry, substantial $\pi-\pi$ overlap, and strong intermolecular S-S interactions of TTF and the dithiolate ligands to enhance conductivity [10]. It was therefore previously supposed that crystallinity was a requirement for conductivity, and as important a feature as those pertaining directly to charge transfer like $\pi-\pi$ overlap. However, the recent discovery of an *amorphous* material exhibiting exceptional conductivity even at room temperature has shaken this supposition and offered a new perspective on conductivity [11]. Amorphous NiTTFtt demonstrates remarkable conductivity in spite of a completely disordered structure, apparently due to the same properties of $\pi-\pi$ overlap, intermolecular S-S interactions, and delocalization along the chain that drive conductivity in more ordered structures. This discovery does, however, raise questions about the nature of such conductivity and other potential capabilities of this unusual material. While some aspects of the mechanism of conductivity were explored in the initial work, here we seek to explore another facet of these questions by investigating the possibility of exciton condensation in stacked structures of TTF molecules and the molecular analogue of NiTTFtt.

Exciton condensation occurs when electron-hole pairs (excitons) undergo Bose-Einstein-like condensation to a single quantum state. Such condensation is a type of coherent long-range order, specifically an off-diagonal long-range order. Although exciton condensation initially received less attention than other more well-known condensation phenomena like superfluidity of liquid helium [12, 13] and superconductivity [14–17], it has played a

[*] These two authors contributed equally

prominent role in more recent research which has sought to realize and understand this phenomenon [18–37]. Like other condensation phenomena, exciton condensation occurs below a specific critical temperature which, because of the relatively small mass of excitons, is expected to be much higher than that of traditional superconductivity [26]. Exciton condensation also leads to superfluid transport of excitons, which can manifest itself as dissipationless flow of energy [38] or, in bilayer systems, can lead to counter-flow superconductivity [39, 40]. For this reason, in addition to increased stabilization of excitons afforded by two-dimensional structures, bilayer structures have captured significant attention in the recent developments in the study of exciton condensation. Exciton condensation has been shown to occur in a variety of two-dimensional systems including double-layer graphene [24, 35, 36], transition metal dichalcogenides [23], and van der Waals heterostructures [31, 32, 34]. Even in small, molecularly-scaled structures, layered structures have been shown to demonstrate the beginnings of exciton condensation, revealing the possibility of the long-range order associated with exciton condensation in molecular systems [22, 29, 30].

Here, we use a computational signature for exciton condensation to demonstrate an excitonic mechanism in both Bechgaard-like van der Waals TTF layered structures and the molecular analogue of NiTTFtt. In both TTF and NiTTFtt, we find appropriate interlayer distances that maximize the signature of condensation and show that the potential for condensation increases with the size of the system. We show that the amorphous geometry of NiTTFtt may enhance rather than reduce exciton condensation and condensation may occur under experimentally viable conditions. Additionally, our calculations show that the excitonic character is enhanced not only by $\pi - \pi$ interactions, but also by side-to-side overlap and longer chain-lengths. Evidence for an excitonic mechanism in these systems provides insight into possible sources of non-traditional superfluidity in these and related systems. Systems capable of superfluidity through an excitonic mechanism could exhibit enhanced exciton transfer leading to super-efficient energy transfer. By using the characteristics identified here and taking advantage of the susceptibility of the excitonic mechanism to structural modifications, molecular systems chemically tuned for exciton condensation could be discovered and utilized to create materials capable of superfluid energy transport.

II. THEORY

A. Signature of Exciton Condensations:

In 1924, Einstein and Bose first developed a theoretical framework for an ideal gas of bosons, a "Bose-Einstein" gas. When adequately cooled, these bosonic particles condense into a single, low-energy quantum ground state [41, 42], which results in the emergence of superfluid properties [12, 43]. A quantum signature representing the computational determination of the presence and scope of this so-called Bose-Einstein condensation is given by a large eigenvalue of the one-boson reduced density matrix (RDM) [13], which is expressed as

$$ {}^1D^i_j = \langle \Psi | \hat{b}^\dagger_i \hat{b}_j | \Psi \rangle \tag{1} $$

with $|\Psi\rangle$ being an N-boson wavefunction, each number demonstrating both the spatial and spin components of the boson, i, j corresponding to one-boson orbitals in a finite basis set with rank r, and $\hat{b}^\dagger$ and $\hat{b}$ depicting bosonic creation and annihilation operators, respectively. Note that as the eigenvalues of the one-boson RDM can be interpreted as the number of bosons occupying a single bosonic orbital, an eigenvalue exceeding one implies multiple bosons occupy the same quantum state and hence the presence of condensation.

For systems comprised of fermions, however, it is not possible for a macroscopic number of particles to aggregate into a single quantum state [44]. Thus, in an uncorrelated fermion density matrix, the eigenvalues have a maximum value of one. Condensation phenomena in fermionic systems arises due to the correlation of fermion-fermion pairs, which create bosonic quasiparticles that can condense. Condensation of Cooper pairs (i.e., particle-particle pairs) results in the superfluidity of these electron-electron pairs, creating traditional superconductivity [14, 16], the quantum signature of which—independently derived by Yang and Sasaki [45, 46]—is a large eigenvalue in the two-particle reduced density matrix (2-RDM), written as

$$ {}^2D^{i,j}_{k,l} = \langle \Psi | \hat{a}^\dagger_i \hat{a}^\dagger_j \hat{a}_l \hat{a}_k | \Psi \rangle \tag{2} $$

with $|\Psi\rangle$ being an N-fermion wavefunction, each number demonstrating both the spatial and spin components of the fermion, i, j, k, l corresponding to one-fermion orbitals in a finite basis set with rank r, and $\hat{a}^\dagger$ and $\hat{a}$ depicting fermionic creation and annihilation operators, respectively.

Similarly, the condensation of particle-hole pairs (i.e., quasibosonic excitons) into a single quantum state results in exciton condensation. In direct analogy to the large eigenvalue of the 2-RDM being a quantum signature for the condensation of particle-particle (Cooper) pairs, one may expect the signature of exciton (particle-hole) condensation to be a large eigenvalue in the particle-hole RDM [22, 47, 48], which is given by

$$ {}^2G^{i,j}_{k,l} = \langle \Psi | \hat{a}^\dagger_i \hat{a}_j \hat{a}^\dagger_l \hat{a}_k | \Psi \rangle. \tag{3} $$

However, there exists an extraneous large eigenvalue of the particle-hole RDM corresponding to a ground-state-to-ground-state transition. Thus, a modified particle-hole matrix with this unrelated large eigenvalue removed is constructed [22, 47, 48] and is represented as

$$ {}^2\tilde{G}^{i,j}_{k,l} = {}^2G^{i,j}_{k,l} - {}^1D^i_k \, {}^1D^j_l \tag{4} $$

We refer to the largest eigenvalue of this modified particle-hole RDM as λ_G and use this eigenvalue as the signature of the extent of exciton condensation throughout the course of our analysis. The large eigenvalue can be interpreted as the number of excitons occupying a single, particle-hole eigenstate of the modified particle-hole RDM. Therefore, a λ_G value exceeding one indicates more than one exciton condensed into the same particle-hole quantum state, which physically means that the excitons are phase coherent like the bosons in a Bose-Einstein condensation. In this case we say that the λ_G excitons form an exciton condensate.

B. Direct Calculation of the 2-RDM

We use the variational 2-RDM (V2RDM) method to directly calculate the 2-RDM from the molecular structure [49–63]. The particle-hole RDM is calculated from the 2-RDM, as in Eq. 8. We have previously developed V2RDM theory as an advanced electronic structure method capable of capturing strong correlation and applied it to explore a variety of molecular systems with strong correlation effects [8, 62, 64–67]. In contrast to other strong correlation methods like CASSCF, V2RDM avoids calculation of the wave function and instead directly computes the 2-RDM). The 2-RDM contains information about correlation in a molecular system, including information about van der Waals interactions [49, 68].

Due to the pairwise nature of electronic interactions, the energy of a molecule can be expressed a function of the 2-RDM as follows:

$$E = \sum_{i,j,k,l} {}^2K^{i,j}_{k,l}\ {}^2D^{i,j}_{k,l} = \mathrm{Tr}({}^2K\ {}^2D) \tag{5}$$

where ${}^2K$ is the two-electron reduced Hamiltonian matrix:

$${}^2\hat{K} = \frac{1}{N-1}(-\frac{1}{2}\nabla_1^2 - \sum_i \frac{Z_j}{r_{1j}}) + \frac{1}{2}\frac{1}{r_{12}}. \tag{6}$$

The energy must then be minimized as a functional of the 2-RDM subject to N-representability conditions. The ensemble N-representability conditions constrain the 2-RDM to represent an N-electron ensemble density matrix. Basic requirements on the 2-RDM include Hermiticity, normalization, and antisymmetry of the fermions. Here we also apply additional N-representability conditions beyond the basic requirements known as the 2-positivity conditions [51, 59, 63, 69]. The 2-RDM is normalized to have a trace of $N(N-1)$. The 2-positivity conditions, also called the DQG conditions, constrain the two-particle (Eq. 2), two-hole (${}^2Q^{i,j}_{k,l} = \langle\Psi|\hat{a}_i\hat{a}_j\hat{a}_l^\dagger\hat{a}_k^\dagger|\Psi\rangle$), and particle-hole (Eq. 3) reduced density matrices to be positive semidefinite, meaning that all eigenvalues of the matrices must be nonnegative. The DQG conditions can be written in matrix form as:

$$\begin{pmatrix} {}^2D & 0 & 0 \\ 0 & {}^2Q & 0 \\ 0 & 0 & {}^2G \end{pmatrix} \succeq 0. \tag{7}$$

Additionally, the ${}^2D$, ${}^2Q$, and ${}^2G$ matrices are interrelated by linear mappings resulting from rearrangement of the creation and annihilation operators. The optimization is performed by semidefinite programming in which the energy is minimized as a linear functional of the ${}^2D$, ${}^2Q$, and ${}^2G$ matrices subject to the 2-positive constraints that each of these matrices must be positive semidefinite. Because the imposed 2-positive conditions are necessary but not sufficient for N-representability, the minimized energy from a variational 2-RDM calculation is a lower bound to the ground-state energy.

The molecular geometry of tetrathifulvalene (TTF) is obtained via the PubChem database [70], and van der Waal structures of TTF layers are constructed through vertical stacking of these TTF subunits at the specified interlayer distances. Molecular geometry for the NiT-TFtt molecular analogue is obtained from Ref. [11] and coordinates of a representative unit are given in the SI.

C. Large Eigenvalue of the Modified G-Matrix

The particle-hole RDM is calculated via a direct mapping from the particle-particle RDM given by

$${}^2G^{i,j}_{k,l} = \delta^{j\,1}_{l} D^{i}_{k} + {}^2D^{i,k}_{j,l} \tag{8}$$

where ${}^1D$ is the one-fermion RDM which is obtained from the ${}^2D$ via contraction and δ is the Kronecker delta function. The modified particle-hole RDM is then obtained via Eq. (4), with the eigenvalues ϵ_i and eigenvectors v_i of this matrix being computed through solving the following eigenvalue equation:

$${}^2\tilde{G}v_i = \epsilon_i v_i \tag{9}$$

The largest eigenvalue (the maximum ϵ_i) is our signature of exciton condensation, which we label λ_G. As discussed in section II A, the eigenvalue λ_G indicates the number of excitons in a single, phase-coherent particle-hole state. When $\lambda_G > 1$, we begin to form a Bose-Einstein condensate of excitons, an exciton condensate. Because the particle-hole RDM corresponds to the ground state, λ_G reveals exciton condensation in the ground state.

D. Visualization of Excitonic Modes

The visualization of the excitonic modes corresponding to maximum exciton condensate character is accomplished by constraining the location of the excitonic particle to a given atomic orbital and probing the location of the excitonic hole. Through use of the V2RDM method,

developed by one of the authors and implemented in the Quantum Chemistry package in Maple, a matrix expressing the canonical molecular orbitals (columns) in terms of atomic orbitals (rows)—denoted $M_{\mathrm{MO,AO}}$—is obtained. This matrix is then manipulated by

$$M_{\mathrm{AO,MO}} = (M^T_{\mathrm{MO,AO}})^{-1} \tag{10}$$

in order to express the atomic orbitals (columns) in terms of the canonical molecular orbitals (rows), and the submatrix of $M_{\mathrm{AO,MO}}$ corresponding to the active orbitals is then isolated and denoted as $M^{submat}_{\mathrm{AO,MO}}$. The eigenvector of the modified particle-hole reduced density matrix corresponding to the largest eigenvalue, v_{max} is obtained from the spin-adapted ${}^2\tilde{G}$ matrix according to Eq. (9) and reshaped into a matrix in the basis of active molecular orbitals, V_{max}. Then,

$$(M^{\mathrm{submat}}_{\mathrm{AO,MO}})(V_{\mathrm{max}})(M^{\mathrm{submat}}_{\mathrm{AO,MO}})^T \tag{11}$$

is performed to result in a matrix in which specified particle atomic orbitals are represented in terms of coefficients corresponding to the hole contributions to other molecular orbitals. Visualization tools in Maple can then be utilized to provide a visual representation of a probabilistic hole location for the specified particle location for a given excitonic mode.

III. RESULTS

Broadly, the term exciton condensation refers to formation of a coherent quantum state of excitons. However, because the nature of excitons is wide-ranging, the nature of exciton condensation is similarly varied. For instance, exciton condensation can occur in excitons trapped in a quantum well, where the excitons act like a dilute gas and condensation is similar to that of bosons in an atomic gas [32, 34, 37, 71]. Excitons coupled to photons to form polaritons can also condense and the resulting condensate is sometimes referred to as an exciton condensate, despite being distinct from the former case [72]. In our study, we consider another type of exciton condensation, where excitons are formed between layers of TTF or NiTTFtt molecules. This is similar to exciton condensation in bilayers, in which excitons are formed in the ground state of the system from the pairing of electrons in one layer to holes in the other [19–21, 24, 39]. Our case, in which each exciton forms from the pairing of an electron (or hole) on one molecule with a hole (or electron) on a second molecule, can be viewed as the molecular case of bilayer exciton condensation. This molecular bilayer definition of exciton condensation, like bilayer exciton condensation, depends on the spatial separation of electrons and holes. Like the other realizations of exciton condensation, this realization is fundamentally due to particle-hole correlation. As such, it exhibits the quantum signature for exciton condensation in which there is more than one exciton in the same particle-hole quantum state. With this perspective in mind, we probe the extent of exciton condensation using the computational signature of exciton condensation in the ground electronic states of layered structures of TTF and molecular NiTTFtt.

A. TTF System

As the primary method for controlling the ground-state properties of layered systems—such as Bechgaard salts—is to control the spacing of layers—through chemical means and/or the application of mechanical pressure—in order to alter orbital overlap [1], we probe the extent of exciton condensation—signified by the magnitude of λ_G—between two layers of TTF with varying interlayer distance. Typical interlayer distances in superconducting TTF-related materials are around 3.6-3.8 Å under ambient pressure and compress to shorter distances under high pressure [73]. Interlayer distances are varied from 1.0 to 4.0 Å, and the signature of condensation, λ_G, is calculated in the 6-31g basis using a [12,12] active space. Although TTF as part of many Bechgaard salts and other conductors is often partially oxidized, results presented here utilize neutral TTF. Results showing the influence of charge on exciton condensation—found in the Supplemental Material [74]—indicate that charge can either enhance or dampen the large eigenvalue, and is not necessary to observe a large eigenvalue. Therefore, all calculations utilize neutral TTF unless otherwise specified. As can be seen in Fig. 1a, the TTF bilayer system demonstrates potential for exciton condensation ($\lambda_G > 1$, blue) over a multitude of spatial separations, with the 2.0 Å separation having the maximal signature of exciton condensation—as indicated by the largest eigenvalue. As such, this optimal distance of 2.0 Å is utilized as the interlayer distance throughout all further computations in which other variables are varied, including those demonstrating the effect of layer offset and charge which are found in the Supplemental Material [74]. Note that, for completeness, the extent of particle-particle condensation (λ_D, superconductivity) is probed as well; however, as can be seen from the red data in Fig. 1, no significant particle-particle condensation is observed. Finally, we note that while the chosen separation of 2 Å is shorter than those observed experimentally, we do see additional peaks at more experimentally reasonable values of 2.5 and 3 Å.

In order to visualize this excitonic system, we computationally probe an excitonic density by calculating the probabilistic location of a hole corresponding to a specified particle location—in a specified atomic orbital—for a given exciton. (See the Theory section for more information.) This visualization provides a physical representation of the particle-hole pairing elucidating the multi-layer nature of the exciton condensation. Specifically, in Fig. 1c, for the excitonic mode corresponding to the largest signature of exciton condensation, the prob-

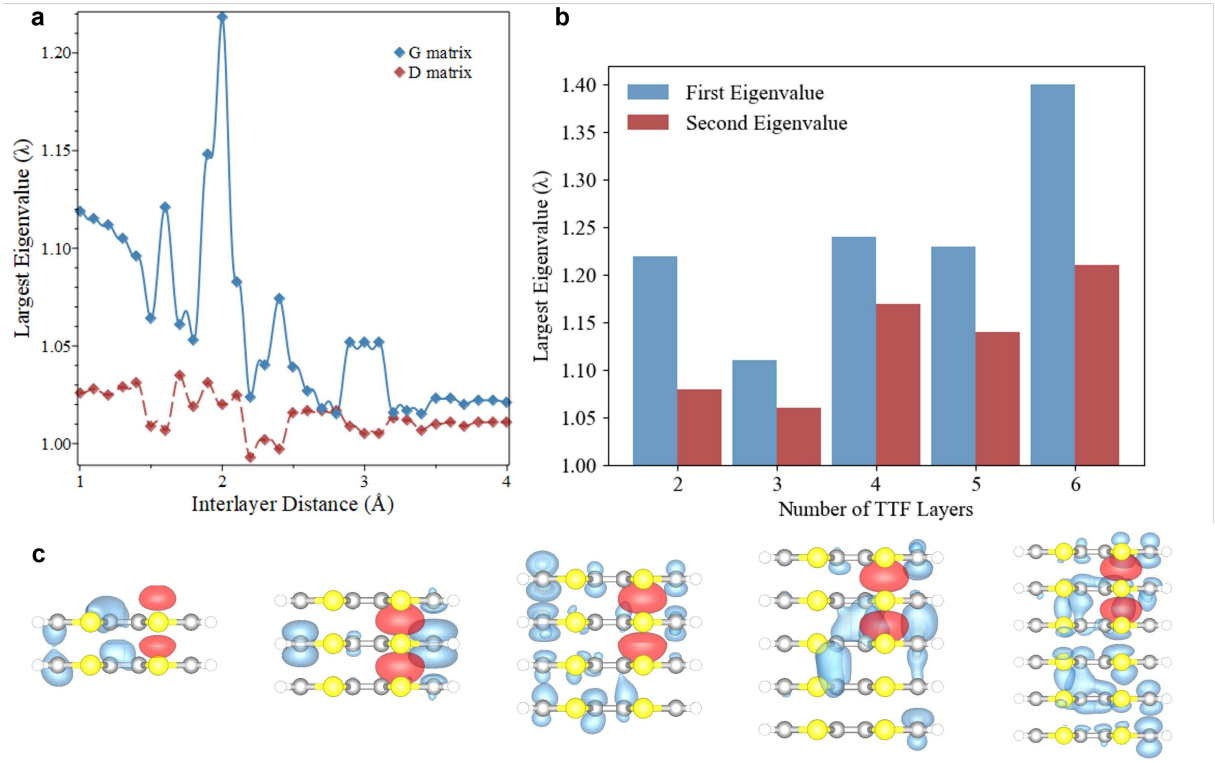

FIG. 1. (a) The largest eigenvalues of the particle-particle density matrix (λ_D, red) and the modified particle-hole density matrix (λ_G, blue) as a function of interlayer distance are given for a bilayer of TTF molecules with no offset. (b) The two largest eigenvalues of the modified particle-hole RDM for TTF layered systems of variable numbers of layers separated by 2.0 Å are shown. (c) Visualization of the exciton where the exciton's particle is constrained to the p_z orbital (shown in red) and where the probabilistic location of the exciton's hole is probed (in blue) for the TTF van der Waals structures composed of 2, 3, 4, 5, and 6 layers (pictured from left to right).

abilistic location of the hole of the exciton (in blue) is shown when the particle of the exciton is constrained to a $4p_z$ orbital of one of the sulfur atoms (in red). From the image corresponding to the bilayer system, the existence of interlayer (as opposed to intralayer) excitons can be readily observed, indicating a possibility of greater excitonic stability.

To explore the behavior of larger van der Waal structure systems and better allow for extrapolated reasoning of excitonic behavior based on system size, we computationally probe the exciton condensate character of multilayer TTF van der Waals structures composed of two-to-six TTF layers. As demonstrated in the previous section, the largest degree of exciton condensation is observed for an interlayer distance of 2.0 Å and an offset distance of 0 Å for the bilayer system. Thus, as the number of TTF layers in the systems is varied, the interlayer and offset distances between each layer are fixed to 2.0 Å and 0 Å, respectively, to allow for direct comparison. (Note that for systems composed of 2, 3, 4, 5, and 6 layers, active spaces of [12,12], [18,18], [24,24], [30,30], and [36,36], are utilized with the 6-31g basis set.)

As can be seen in Fig. 1b, all TTF layered systems probed—from two to six layers—demonstrate character of exciton condensation, evinced by all having an eigenvalue of the modified particle-hole reduced density matrix larger than one. Comparing across all numbers of TTF layers, as the number of even layers increases so does the magnitude of the largest eigenvalue; the same can be said for the odd-layered counterparts, although the magnitude of exciton condensation is lesser for a given system with an odd number of layers than the system one fewer—and hence an even number of—layers.

Another aspect of interest from Fig. 1b is the existence of multiple eigenvalues of the modified particle-hole RDM that exceed one. As the eigenvalues of the modified particle-hole matrix can be interpreted as the number of excitons occupying a certain particle-hole quantum state, these multiple large eigenvalues indicate that there are multiple quantum states containing more than one exciton bosonic quasiparticle and hence multiple quantum states coexisting with character of exciton condensation. These multiple "islands of condensation" [28] coexist within a given system such that the sum of the eigenvalues exceeding one gives an overall measure of the number of excitons existing in a condensate phase, although the condensate character of these excitons do not exist in a single mode. By this metric, excitonic char-

acter increases as the number of layers in the TTF van der Waals structure system is increased with both even and odd numbers of layers supporting this trend. (See the Supplemental Material [74] for a figure showing all eigenvalues that exceed one as well as the sum of all the eigenvalues exceeding one.) As the superfluidity of excitons is likely reliant on a macroscopic number of them existing within the *same* mode, however, this metric is less useful than the signature corresponding to the maximum eigenvalue of the modified particle-hole RDM.

Again, we visualize the exciton density corresponding to the signature of exciton condensation (λ_G) in order to get a sense of the relative delocalization of the excitons in the quantum state corresponding to the largest character of exciton condensation. As can be seen from Fig. 1c, where the particle location for the exciton with the highest character of condensation is specified to a sulfur $4p_z$ orbital (red) and the corresponding hole location is probed (blue), structures of all layer numbers demonstrate significant character of interlayer excitons. By directly comparing the case in which the particle is localized to a sulfur $4p_z$ in the second layer for systems composed of different layers, it is apparent that the hole density is delocalized across the entire stack in each case, with the largest delocalization occurring in the six-layer system, which also corresponds to the largest λ_G of the figures shown. As such, this visualization technique seems to allow for a qualitative analysis of exciton condensation via an analysis of delocalization when the same atomic orbitals are compared.

B. NiTTFtt

By examining interactions and correlation in a molecular model of NiTTFtt Xie et al. [11] uncovered structural factors contributing to the material's unusual conductivity; we use the same molecular model to examine molecular exciton condensation in NiTTFtt by calculating the signature of exciton condensation, λ_G. Molecular geometries, including layer shifts and stacking, of our molecular model are taken from the experimentally determined structure in Ref. [11] and interlayer distances are selected centered around experimentally predicted S-S distances. Most calculations are performed using variational 2-RDM theory (V2RDM); however, some complete active space self-consistent field (CASSCF) calculations are performed for smaller systems to confirm V2RDM results. Due to the large computational cost of CASSCF calculations, only specified calculations are performed with CASSCF and V2RDM is used for all others.

As with TTF, the interlayer distance between layers of NiTTFtt has important implications for the properties of the material. We therefore examine the signature of condensation in a bilayer dimer of NiTTFtt over a range of interlayer distances from 2.5 to 4.25 Å, with an offset between layers of 1.0 Å. Figure 2a shows a plot of S-S distance versus the signature of exciton condensation. The plot shows the distance in S-S distance rather than interlayer distance as demonstrated by Figure 3; this metric is more commonly used in experimental measurements and descriptions of TTF structures, and more accurately describes the important S-S interactions in NiTTFtt. A similar plot for dimers with no offset can be found in the Supplemental Material [74]; however, only results for shifted structures are presented here as the shifted geometry corresponds more closely to the proposed experimental geometry. The blue line shows eigenvalues calculated with V2RDM and the red line shows eigenvalues calculated with CASSCF. The 6-31g basis set and [12,12] active space is used with both methods. Results from the two methods are consistent, as both V2RDM and CASSCF demonstrate eigenvalues greater than one for dimers over the range of distances, with lower magnitudes of eigenvalues at both the short and long ranges of S-S distance and a peak in the center. The gray shaded region on the plot represents the approximate experimental interlayer distance between 3.4 and 3.7 Å, as reported by Ref. [11]. Interestingly, the maximum eigenvalues indicating the greatest character of exciton condensation occur in this region for both V2RDM and CASSCF, with peaks near 1.28. This is significant as it indicates that the potential for exciton condensation is maximized in these structures under the experimental conditions, meaning at ambient pressure.

We further consider the relative shift between layers as a means of mimicking the amorphous structure of bulk NiTTFtt by probing the signature of exciton condensation in shifted two- and three-chain dimers of NiTTFtt. The importance of relative shift between layers to exciton condensation is emphasized in Fig. 2b, which shows results for two-chain and three-chain dimers (see Fig. 2c for structures) with no shift, parallel shift of 1.75 Å, and perpendicular shift of 0.75 Å. In this case, the interlayer distance is 3.55 Å and calculations are performed with the 6-31g* basis set and an [8,8] active space for two-chain and a [12,12] active space for three-chain dimers. The interlayer distance falls within the range of experimental distances indicated by the shaded region of Fig. 2a and the methods give quantitatively similar results to the previous methods used to examine interlayer distance. Additionally, in previous work [29] we showed that λ_G is qualitatively consistent between basis sets for layers of benzene, and the results we calculated using the larger 6-31g* basis set are consistent with those in the 6-31g basis set. The results reveal that the greatest character of exciton condensation occurs for layers shifted parallel to one another, although a perpendicular shift also increases the eigenvalue relative to the unshifted dimer. This suggests that the amorphous structure of NiTTFtt may actually enhance excitonic character. Additionally, the larger three-chain dimers show notably higher eigenvalues than the two-chain dimers, indicating that extending the length of the system increases the degree of exciton condensation. In fact, for the three-chain dimer, a parallel shift yields an eigenvalue of almost 1.7,

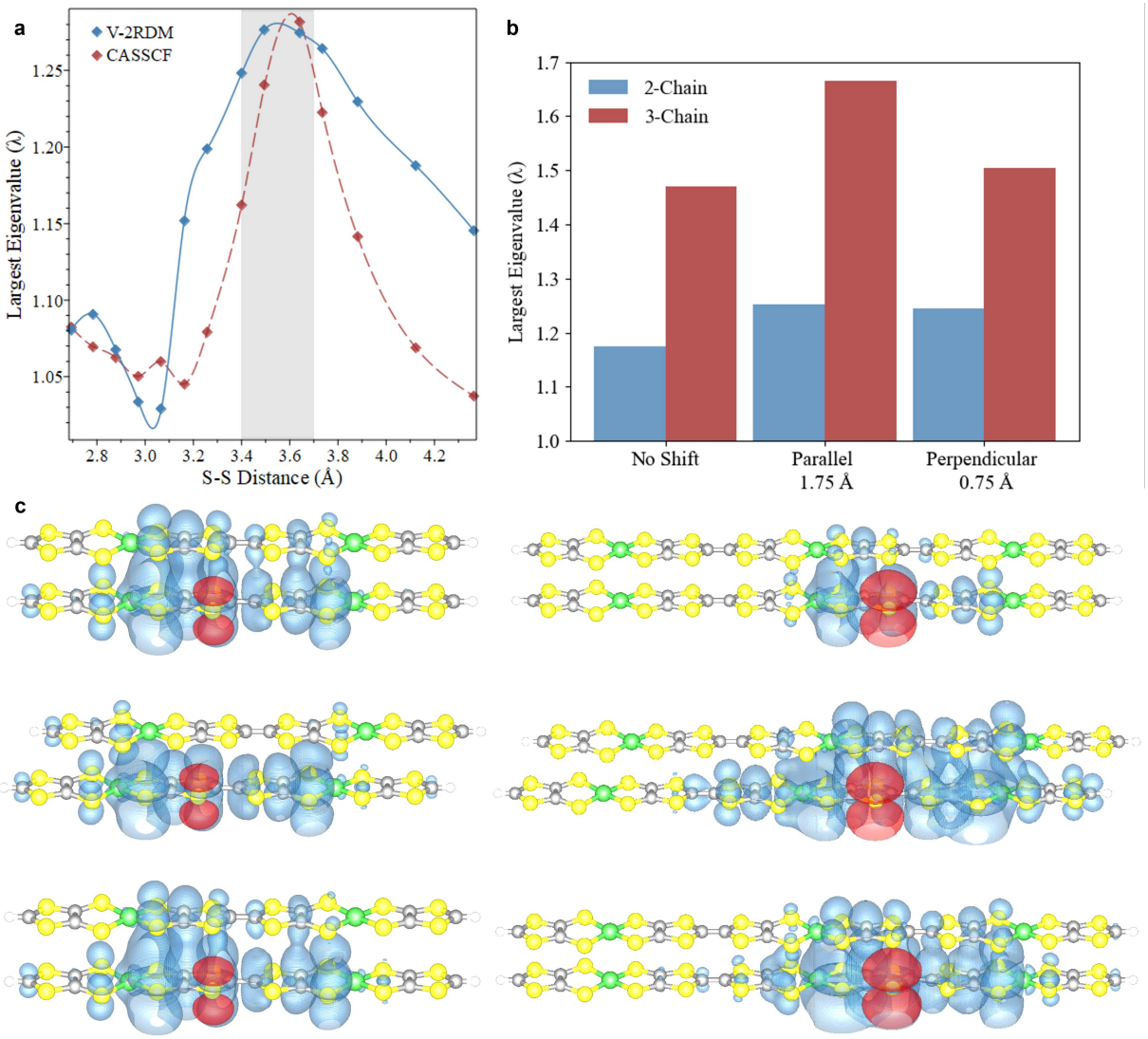

FIG. 2. (a) Plot of S-S distance versus eigenvalues for NiTTFtt molecular dimers, with layers offset parallel by 1 Å. The gray shaded region corresponds to the approximate experimental S-S distance. (b) The calculated eigenvalues for NiTTFtt dimers with an interlayer distance of 3.55 Å and relative shift as indicated. Two-chain dimers are shown in (c) on the left and 3-chain dimers are shown on the right. (c) Left: Exciton densities for the 2-chain with no shift (top), parallel shift of 1.75 Å (middle), and perpendicular shift of 0.75 Å (bottom). Right: Exciton densities for the 3-chain with no shift (top), parallel shift of 1.75 Å (middle), and perpendicular shift of 0.75 Å (bottom).

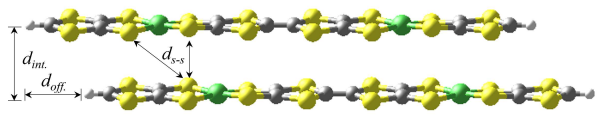

FIG. 3. Demonstrating the offset, interlayer, and S-S distances for a bilayer of NiTTFtt

demonstrating growth compared to the parallel shifted two-chain dimer ($\lambda_G = 1.25$). The delocalization of the exciton condensate is probed by modeling the exciton density with the particle constrained to the $4p_z$ orbital of a sulfur atom, as with TTF. Fig. 2c shows the exciton densities for the two-chain and three-chain dimers, demonstrating that the hole is delocalized between both layers of the dimer, therefore neither parallel nor perpendicular shifts inhibit interlayer delocalization. Additionally, the exciton densities reveal that there is greater intralayer delocalization in parallel-shifted structures and along longer NiTTFtt chains.

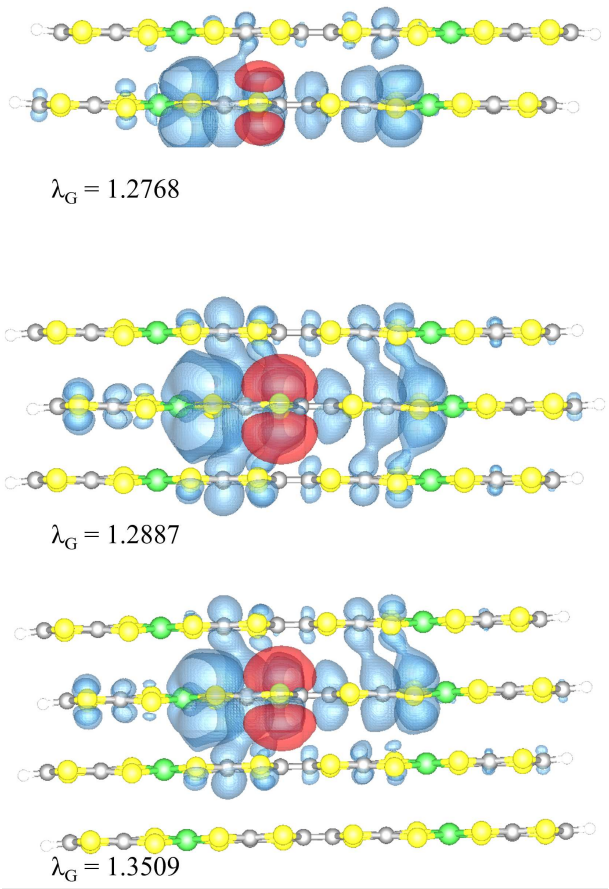

FIG. 4. Exciton densities and eigenvalues for NiTTFtt stacks of two layers (top), three layers (middle), and four layers (bottom), with interlayer distances of 3.35 Å and alternating parallel offsets of 1 Å.

C. Extended Systems

To further explore the influence of system size on the degree of exciton condensation, we compute the signature of exciton condensation for several extended NiTTFtt systems. The first of these are vertical stacks of molecular units, with layers stacked 3.35 Å apart and alternating parallel shifts of 1 Å. This geometry was chosen as it corresponds to the maximum extent of condensation from Fig. 2a. Figure 4 shows results for two-, three-, and four-layer stacks calculated with [12,12], [18,18], and [24,24] active spaces, respectively, using V2RDM with the 6-31g basis set. As the number of layers in the stack increases, so does the magnitude of the eigenvalue, although a greater increase occurs between the three- ($\lambda_G = 1.29$) and four-layer ($\lambda_G = 1.35$) stacks than the two- ($\lambda_G = 1.28$) and three-layer ($\lambda_G = 1.29$) stacks, which are approximately equal, similar to the trend we observe in TTF. Due to the size of NiTTFtt, results could not be obtained for larger numbers of layers; however, we expect results to be consistent with the trend noted for TTF stacks showing an increase with the number of layers and a greater increase for even-layered than odd-layered systems. Figure 4 also shows exciton densities for each stack, again with the particle constrained to the $4p_z$ orbital of a sulfur atom, revealing that as with dimers, there is delocalization of the density within and between NiTTFtt layers.

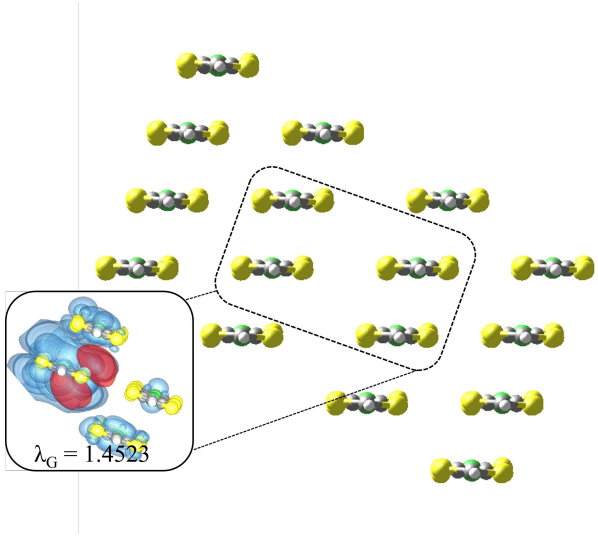

FIG. 5. A modeled crystal-like structure for NiTTFtt; the inset shows the calculated exciton density and eigenvalue for a four molecule fragment.

In addition to vertical stacking, we examine an extended NiTTFtt system based on a modeled crystalline structure. Although synthesized NiTTFtt is amorphous, the modeled structure illustrates the effect of extending the system both vertically and side-to-side. The modeled system shown in Fig. 5 consists of stacked NiTTFtt molecules spaced 3.35 Å apart with a perpendicular shift and alternating parallel shifts. Stacks are placed side-by-side to form an extended structure. The inset of Fig. 5 shows results for a four-molecule fragment of this structure, which has an eigenvalue of 1.45 and exciton density delocalized over all four molecules. (A two molecule, vertically stacked fragment has an eigenvalue of 1.22). Despite containing the same number of NiTTFtt units, the fragment has a larger eigenvalue than the vertical stack of four molecules, indicating that both vertical and side-to-side interactions enhance exciton condensation.

Exciton condensation is known to occur below specific critical temperatures. An estimate of the maximum critical temperature for exciton condensation can be made by taking 10-15% of the exciton binding energy [34, 75]. We calculate exciton binding energy as the energy required to disperse the condensate, making the value an estimated lower bound on the binding energy. Further details of the methodology for calculating the binding energy will be presented in future work. For molecular NiTTFtt we

calculate an exciton binding energy of at least 22 meV for a two-chain dimer with an interlayer distance of 3.35 Å and a 1 Å shift, yielding estimated critical temperatures around 26 K.

IV. DISCUSSION AND CONCLUSIONS

We demonstrate the existence of an excitonic mechanism in Bechgaard-like van der Waals stacks of TTF and molecular NiTTFtt using a computational signature of exciton condensation. We show that the potential for exciton condensation is dependent on the interlayer spacing or S-S spacing of the stacked structures. Significantly, the greatest character of exciton condensation occurs in the NiTTFtt stacks in the region of S-S spacing that is found in the synthesized experimental structure. This suggests that the excitonic mechanism could be realized at ambient pressure without subjecting the material to high pressures. We additionally show that in dimers of NiTTFtt that are shifted either parallel or perpendicularly to mimic variations found in the amorphous nature of the experimental structure, there is increased excitonic character relative to unshifted dimers, meaning that the amorphous structure of NiTTFtt may enhance the excitonic character relative to a more ordered structure. Lastly, we demonstrate the potential for realization of greater exciton condensation in extended systems as we observe that in both TTF and NiTTFtt systems, the excitonic character increases with the number of layers in a stack. In TTF stacks, we show that the increase in excitonic character is greater for systems of even-numbered layers than odd-numbered layers, a trend we expect to observe in NiTTFtt as well. Moreover, we demonstrate that excitonic character is enhanced in NiTTFtt not only in larger vertical stacks, but in dimers of longer chain length and a fragment of a modeled crystal structure that introduces horizontal stacking. Thus, the excitonic mechanism must depend on a combination of $\pi - \pi$ stacking, chain-length, and side-to-side S-S interactions. Although the eigenvalues do not necessarily demonstrate exciton condensation in the macroscopic sense, the presence of an eigenvalue greater than one is a purely strongly correlated effect not observed in a typical molecular system. Moreover, the observation of the large eigenvalue in the molecular analogue of a material like NiTTFtt is the critical seed of macroscopic exciton condensation. The increase in the large eigenvalue in the extended systems suggests that the growth may continue as the system becomes large, potentially leading to macroscopic exciton condensation in materials-scale NiTTFtt polymers. While the large eigenvalue signature we observe does not guarantee exciton condensation in the material, it is a necessary condition for long-range order and the beginnings of exciton condensation.

Our results offer significant insight into the excitonic mechanism present in NiTTFtt. While we cannot definitively attribute the unusual conductive characteristics of NiTTFtt to exciton condensation, our analysis suggests that an excitonic mechanism for such conductivity is possible. Even in the absence of a definitive connection to the exceptional conductivity of NiTTFtt, however, our results nevertheless represent a step forward in the pursuit of long-range coherence in molecularly constructed materials. Our results provide evidence of long-range coherence in a molecularly-scaled fragments of NiTTFtt and TTF, which opens the door not only to the possibility of realizing exciton condensation in macroscopic systems of NiTTFtt, but also to potentially observing long-range coherence in molecular systems. Such molecular long-range coherence could prove important to understanding and utilizing efficient exciton transfer in a variety of natural and synthetic systems.

A search for highly-conductive materials that maintain their conductivity at high temperatures has long been central in the hope for designing highly-efficient wires and electronics. However, such properties have previously been relegated to the regimes of low temperatures and high magnetic fields. Here we explore a molecular analogue of a recently synthesized NiTTFtt polymer that has been experimentally shown to support anomalous conductivity under more-favorable conditions. The analogue, we computationally show, exhibits a large eigenvalue in the particle-hole reduced density matrix—a signature for exciton condensation, possibly elucidating the mechanism for the the conductivity in the experimental polymer.

Supplemental Material:
Results contained in the Supplemental Material: variation of layer offset in TTF, variation of charge on TTF layers, NiTTFtt with no layer offset, variation of charge on NiTTFtt layers, and XYZ coordinates of NiTTFtt dimer.

ACKNOWLEDGMENTS

Acknowledgments: D.A.M. and J.S.A. gratefully acknowledge the Department of Energy, Office of Basic Energy Sciences, Grant DE-SC0019215. D.A.M. also acknowledges the ACS-PRF Grant 61644-ND6. The authors also thank Jan-Niklas Boyn for assistance with the molecular geometries of NiTTFtt.

Author contributions. D.A.M. and J.S.A. conceived of the project. A.O.S., J.K., and L.M.S. performed the computations. All of the authors analyzed the data and contributed to writing the manuscript.

Competing interests. The authors do not have competing interests.

Materials & Correspondence. D.A.M. is the corresponding author at damazz@uchicago.edu.

[1] S. Brown, Organic Superconductors: The Bechgaard Salts and Relatives, Phys. C (Amsterdam, Neth.) **514**, 279 (2015).

[2] D. Jérome, A. Mazaud, M. Ribault, and K. Bechgaard, Superconductivity in a synthetic organic conductor $(TMTSF)_2PF_6$, J. Phys., Lett **41**, 95 (1980).

[3] M. Lang and J. Müller, Organic superconductors, in *The Physics of Superconductors: Vol. II. Superconductivity in Nanostructures, High-Tc and Novel Superconductors, Organic Superconductors*, edited by K. H. Bennemann and J. B. Ketterson (Springer Berlin Heidelberg, 2004) pp. 453–554.

[4] D. Jèrome, Organic conductors: From charge density wave TTF-TCNQ to superconducting $(TMTSF)_2PF_6$, Chem. Inform. **36**, 10.1002/chin.200507281 (2005).

[5] A. G. Lebed, *The Physics of Organic Superconductors and Conductors* (Springer, 2008).

[6] H. Kobayashi, A. Kobayashi, Y. Sasaki, G. Saito, and H. Inokuchi, The crystal structure of $(TMTTF)_2ReO_4$, Bull. Chem. Soc. Jpn. **57**, 2025 (1984).

[7] L. Valade, D. de Caro, C. Faulmann, and K. Jacob, TTF[Ni(dmit)2]2: From single-crystals to thin layers, nanowires, and nanoparticles, Coord. Chem. Rev. **308**, 433 (2016).

[8] J. Xie, J.-N. Boyn, A. S. Filatov, A. J. McNeece, D. A. Mazziotti, and J. S. Anderson, Redox, transmetalation, and stacking properties of tetrathiafulvalene-2,3,6,7-tetrathiolate bridged tin, nickel, and palladium compounds, Chem. Sci. **11**, 1066 (2020).

[9] A. Kobayashi, H. Tanaka, and H. Kobayashi, Molecular design and development of single-component molecular metals, J. Mater. Chem. **11**, 2078 (2001).

[10] A. Kobayashi, E. Fujiwara, and H. Kobayashi, Single-component molecular metals with extended-TTF dithiolate ligands, Chem. Rev. **104**, 5243 (2004).

[11] J. Xie, S. Ewing, J.-N. Boyn, A. S. Filatov, B. Cheng, T. Ma, G. L. Grocke, N. Zhao, R. Itani, X. Sun, H. Cho, Z. Chen, K. W. Chapman, S. N. Patel, D. V. Talapin, J. Park, D. A. Mazziotti, and J. S. Anderson, Intrinsic glassy-metallic transport in an amorphous coordination polymer, Nature **611**, 479 (2022).

[12] L. Tisza, The theory of liquid helium, Phys. Rev. **72**, 838 (1947).

[13] O. Penrose and L. Onsager, Bose-Einstein condensation and liquid helium, Phys. Rev. **104**, 576 (1956).

[14] J. Bardeen, L. N. Cooper, and J. R. Schrieffer, Theory of superconductivity, Phys. Rev. **108**, 1175 (1957).

[15] J. M. Blatt, Electron pairs in the theory of superconductivity, Prog. Theor. Phys. **23**, 447 (1960).

[16] P. W. Anderson, Twenty-five years of high-temperature superconductivity – a personal review, J. Phys.: Conf. Ser. **449**, 012001 (2013).

[17] A. P. Drozdov, P. P. Kong, V. S. Minkov, S. P. Besedin, M. A. Kuzovnikov, S. Mozaffari, L. Balicas, F. F. Balakirev, D. E. Graf, V. B. Prakapenka, E. Greenberg, D. A. Knyazev, M. Tkacz, and M. I. Eremets, Superconductivity at 250 K in lanthanum hydride under high pressures, Nature **569**, 528 (2019).

[18] J. M. Blatt, K. W. Böer, and W. Brandt, Bose-Einstein condensation of excitons, Phys. Rev. **126**, 1691 (1962).

[19] M. Kellogg, J. P. Eisenstein, L. N. Pfeiffer, and K. W. West, Vanishing Hall resistance at high magnetic field in a double-layer two-dimensional electron system, Phys. Rev. Lett. **93**, 036801 (2004).

[20] E. Tutuc, M. Shayegan, and D. A. Huse, Counterflow measurements in strongly correlated GaAs hole bilayers: Evidence for electron-hole pairing, Phys. Rev. Lett. **93**, 36802 (2004).

[21] D. V. Fil and S. I. Shevchenko, Electron-hole superconductivity (review), Low Temp. Phys. **44**, 867 (2018).

[22] S. Safaei and D. A. Mazziotti, Quantum signature of exciton condensation, Phys. Rev. B **98**, 045122 (2018).

[23] A. Kogar, M. S. Rak, S. Vig, A. A. Husain, F. Flicker, Y. I. Joe, L. Venema, G. J. MacDougall, T. C. Chiang, E. Fradkin, J. van Wezel, and P. Abbamonte, Signatures of exciton condensation in a transition metal dichalcogenide, Science **358**, 1314 (2017).

[24] X. Liu, K. Watanabe, T. Taniguchi, B. I. Halperin, and P. Kim, Quantum Hall drag of exciton condensate in graphene, Nat. Phys. **13**, 746 (2017).

[25] D. Varsano, S. Sorella, D. Sangalli, M. Barborini, S. Corni, E. Molinari, and M. Rontani, Carbon nanotubes as excitonic insulators, Nat. Commun. **8**, 1461 (2017).

[26] M. S. Fuhrer and A. R. Hamilton, Chasing the exciton condensate, Phyics **9**, 80 (2016).

[27] L. M. Sager, S. Safaei, and D. A. Mazziotti, Potential coexistence of exciton and fermion-pair condensations, Phys. Rev. B **101**, 081107 (2020).

[28] L. M. Sager, S. E. Smart, and D. A. Mazziotti, Preparation of an exciton condensate of photons on a 53-qubit quantum computer, Phys. Rev. Res. **2**, 043205 (2020).

[29] A. O. Schouten, L. M. Sager, and D. A. Mazziotti, Exciton condensation in molecular-scale van der Waals stacks, J. Phys. Chem. Lett. **12**, 9906 (2021).

[30] L. M. Sager, A. O. Schouten, and D. A. Mazziotti, Beginnings of exciton condensation in coronene analog of graphene double layer, J. Chem. Phys. **156**, 154702 (2022).

[31] Z. Wang, D. A. Rhodes, K. Watanabe, T. Taniguchi, J. C. Hone, J. Shan, and K. F. Mak, Evidence of high-temperature exciton condensation in two-dimensional atomic double layers, Nature **574**, 76 (2019).

[32] L. Sigl, F. Sigger, F. Kronowetter, J. Kiemle, J. Klein, K. Watanabe, T. Taniguchi, J. J. Finley, U. Wurstbauer, and A. W. Holleitner, Signatures of a degenerate many-body state of interlayer excitons in a van der Waals heterostack, Phys. Rev. Res. **2**, 042044 (2020).

[33] L. Ma, P. X. Nguyen, Z. Wang, Y. Zeng, K. Watanabe, T. Taniguchi, A. H. MacDonald, K. F. Mak, and J. Shan, Strongly correlated excitonic insulator in atomic double layers, Nature **598**, 585 (2021).

[34] M. M. Fogler, L. V. Butov, and K. S. Novoselov, High-temperature superfluidity with indirect excitons in van der Waals heterostructures, Nat. Commun. **5**, 4555 (2014).

[35] H. Min, R. Bistritzer, J.-J. Su, and A. MacDonald, Room-temperature superfluidity in graphene bilayers, Phys. Rev. B **78**, 121401 (2008).

[36] J. J. Su and A. H. MacDonald, Spatially indirect exciton condensate phases in double bilayer graphene, Phys. Rev. B **95**, 045416 (2017).

[37] L. V. Butov, A. Zrenner, G. Abstreiter, G. Böhm, and

G. Weimann, Condensation of indirect excitons in coupled AlAs/GaAs quantum wells, Phys. Rev. Lett. **73**, 304 (1994).
[38] L. V. Keldysh, Coherent states of excitons, Phys.-Uspekhi **60**, 1180 (2017).
[39] J. P. Eisenstein and A. H. MacDonald, Bose-Einstein condensation of excitons in bilayer electron systems, Nature **432**, 691 (2004).
[40] J.-J. Su and A. H. MacDonald, How to make a bilayer exciton condensate flow, Nat. Phys. **4**, 799 (2008).
[41] S. N. Bose and A. Einstein, Planck's law and light quantum hypothesis, Zeitscrift für Physik **26**, 178 (1924).
[42] A. Einstein, Quantentheorie des einatomigen idealen gases, K.P.A.W. , 261 (1924).
[43] F. London, On Bose-Einstein condensation, Phys. Rev. **54**, 947 (1938).
[44] W. Pauli, The connection between spin and statistics, Phys Rev **58**, 716 (1940).
[45] C. N. Yang, Concept of off-diagonal long-range order and the quantum phases of liquid He and of superconductors, Rev. Mod. Phys. **34**, 694 (1962).
[46] F. Sasaki, Eigenvalues of fermion density matrices, Phys. Rev. **138**, B1338 (1965).
[47] C. Garrod and M. Rosina, Particle-hole matrix: Its connection with the symmetries and collective features of the ground state, J. Math. Phys. **10**, 1855 (1969).
[48] W. Kohn and D. Sherrington, Two kinds of bosons and bose condensates, Rev. Mod. Phys. **42**, 1 (1970).
[49] D. A. Mazziotti, *Reduced-density-matrix Mechanics: With Application to Many-electron Atoms and Molecule*, Vol. 134 (Adv. Chem. Phys., Wiley, New York, 2007).
[50] D. A. Mazziotti, Two-electron reduced density matrix as the basic variable in many-electron quantum chemistry and physics, Chem. Rev. **112**, 244 (2012).
[51] D. A. Mazziotti, Pure-N-representability conditions of two-fermion reduced density matrices, Phys. Rev. A **94**, 10.1103/PhysRevA.94.032516 (2016).
[52] D. A. Mazziotti, Large-scale semidefinite programming for many-electron quantum mechanics, Phys. Rev. Lett. **106**, 083001 (2011).
[53] J. Cioslowski, ed., *Many-electron Densities and Reduced Density Matrices*, 1st ed. (Springer New York, NY, 2012).
[54] M. Nakata, H. Nakatsuji, M. Ehara, M. Fukuda, K. Nakata, and K. Fujisawa, Variational calculations of fermion second-order reduced density matrices by semidefinite programming algorithm, J. Chem. Phys. **114**, 8282 (2001).
[55] D. A. Mazziotti, Realization of quantum chemistry without wave functions through first-order semidefinite programming, Phys. Rev. Lett. **93**, 213001 (2004).
[56] Z. Zhao, B. J. Braams, M. Fukuda, M. L. Overton, and J. K. Percus, The reduced density matrix method for electronic structure calculations and the role of three-index representability conditions, J. Chem. Phys. **120**, 2095 (2004).
[57] E. Cances, G. Stoltz, and M. Lewin, The electronic ground-state energy problem: A new reduced density matrix approach, J. Chem. Phys. **125**, 064101 (2006).
[58] G. Gidofalvi and D. A. Mazziotti, Active-space two-electron reduced-density-matrix method: Complete active-space calculations without diagonalization of the n-electron Hamiltonian, J. Chem. Phys. **129**, 134108 (2008).
[59] N. Shenvi and A. F. Izmaylov, Active-space N-representability constraints for variational two-particle reduced density matrix calculations, Phys. Rev. Lett. **105**, 10.1103/physrevlett.105.213003 (2010).
[60] D. A. Mazziotti, Structure of fermionic density matrices: Complete N-representability conditions, Phys. Rev. Lett. **108**, 263002 (2012).
[61] B. Verstichel, H. V. Aggelen, W. Poelmans, and D. V. Neck, Variational two-particle density matrix calculation for the hubbard model below half filling using spin-adapted lifting conditions, Phys. Rev. Lett. **108**, 10.1103/physrevlett.108.213001 (2012).
[62] A. W. Schlimgen, C. W. Heaps, and D. A. Mazziotti, Entangled electrons foil synthesis of elusive low-valent vanadium oxo complex, J. Phys. Chem. Lett. **7**, 627 (2016).
[63] M. Piris, Global method for electron correlation, Phys. Rev. Lett. **119**, 10.1103/physrevlett.119.063002 (2017).
[64] J.-N. Boyn, J. Xie, J. S. Anderson, and D. A. Mazziotti, Entangled electrons drive a non-superexchange mechanism in a cobalt quinoid dimer complex, J. Phys. Chem. Lett. **11**, 4584 (2020).
[65] S. Ewing and D. A. Mazziotti, Correlation-driven phenomena in periodic molecular systems from variational two-electron reduced density matrix theory, J. Chem. Phys. **154**, 214106 (2021).
[66] A. R. McIsaac and D. A. Mazziotti, Ligand non-innocence and strong correlation in manganese superoxide dismutase mimics, Phys. Chem. Chem. Phys. **19**, 4656 (2017).
[67] A. Kawamura, J. Xie, J.-N. Boyn, K. A. Jesse, A. J. McNeece, E. A. Hill, K. A. Collins, J. A. Valdez-Moreira, A. S. Filatov, J. W. Kurutz, D. A. Mazziotti, and J. S. Anderson, Reversible switching of organic diradical character via iron-based spin-crossover, J. Am. Chem. Soc. **142**, 17670 (2020).
[68] O. Werba, A. Raeber, K. Head-Marsden, and D. A. Mazziotti, Signature of van der Waals interactions in the cumulant density matrix, Phys. Chem. Chem. Phys. **21**, 23900 (2019).
[69] A. J. Coleman, Structure of fermion density matrices, Rev. Mod. Phys. **35**, 668 (1963).
[70] Pubchem compound summary for cid 99451, tetrathiafulvalene.
[71] L. V. Butov, Exciton condensation in coupled quantum wells, Solid State Commun. **127**, 89 (2003).
[72] J. Kasprzak, M. Richard, S. Kundermann, A. Baas, P. Jeambrun, J. M. J. Keeling, F. M. Marchetti, M. H. Szymanska, R. André, J. L. Staehli, V. Savona, P. B. Littlewood, B. Deveaud, and L. S. Dang, Bose-Einstein condensation of exciton polaritons, Nature **443**, 409 (2006).
[73] R. P. Shibaeva and E. B. Yagubskii, Molecular conductors and superconductors based on trihalides of BEDT-TTF and some of its analogues, Chem. Rev. **104**, 5347 (2004).
[74] See Supplemental Material at url for variation of layer offset in TTF, variation of charge on TTF layers, NiTTFtt with no layer offset, variation of charge on NiTTFtt layers, XYZ coordinates of NiTTFtt dimer as well as Refs. [76–81].
[75] P. H. Handel and C. Kittel, Van der Waals interactions and exciton condensation, Proc. Natl. Acad. Sci. **68**, 3120 (1971).
[76] M. R. Bryce, Recent progress on conducting organic charge-transfer salts, Chem. Soc. Rev. **20**, 355 (1991).
[77] Y. Okano, B. Zhou, H. Tanaka, T. Adachi, Y. Ohishi,

M. Takata, S. Aoyagi, E. Nishibori, M. Sakata, A. Kobayashi, and H. Kobayashi, High-pressure (up to 10.7 GPa) crystal structure of single-component molecular metal $[Au(tmdt)_2]$, J. Am. Chem. Soc. **131**, 7169 (2009).

[78] H. Cui, H. Kobayashi, S. Ishibashi, M. Sasa, F. Iwase, R. Kato, and A. Kobayashi, A single-component molecular superconductor, J. Am. Chem. Soc. **136**, 7619 (2014).

[79] L. Valade, D. de Caro, C. Faulmann, and K. Jacob, $TTF[Ni(dmit)_2]_2$: From single-crystals to thin layers, nanowires, and nanoparticles, Coord. Chem. Rev. **308**, 433 (2016).

[80] B. Zhou, S. Ishibashi, T. Ishii, T. Sekine, R. Takehara, K. Miyagawa, K. Kanoda, E. Nishibori, and A. Kobayashi, Single-component molecular conductor $[Pt(dmdt)_2]$—a three-dimensional ambient-pressure molecular Dirac electron system, Chem. Commun. **55**, 3327 (2019).

[81] P. Foury-Leylekian, S. Petit, I. Mirebeau, A. G., M. de Souza, M. Lang, E. Ressouche, A. Moradpour, and J.-P. Pouget, Low-temperature structural effects in the $(TMTSF)_2PF_6$ and AsF_6 bechgaard salts, Phys. Rev. B **88**, 024105 (2013).